

See discussions, stats, and author profiles for this publication at: <https://www.researchgate.net/publication/3011402>

Efficient radar target recognition using the MUSIC algorithm and invariant feature

Article in IEEE Transactions on Antennas and Propagation · April 2002

DOI: 10.1109/8.999623 · Source: IEEE Xplore

CITATIONS

143

3 authors, including:



Kyung-Tae Kim
Inje University Paik Hospital
180 PUBLICATIONS 1,487 CITATIONS

[SEE PROFILE](#)

READS

1,348

H.-T. Kim
Pohang University of Science and Technology
103 PUBLICATIONS 1,627 CITATIONS

[SEE PROFILE](#)

Efficient Radar Target Recognition Using the MUSIC Algorithm and Invariant Features

Kyung-Tae Kim, Dong-Kyu Seo, and Hyo-Tae Kim

Abstract—In this paper, an efficient technique is developed to recognize target type using one-dimensional range profiles. The proposed technique utilizes the Multiple Signal Classification algorithm to generate superresolved range profiles. Their central moments are calculated to provide translation-invariant and level-invariant feature vectors. Next, the computed central moments are mapped into values between zero and unity, followed by a principal component analysis to eliminate the redundancy of feature vectors. The obtained features are classified based on the Bayes classifier, which is one of the statistical classifiers. Recognition results using five different aircraft models measured at compact range are presented to assess the effectiveness of the proposed technique, and they are compared with those of the conventional range profiles obtained by inverse fast Fourier transform.

Index Terms—Feature extraction, radar signal processing, radar target recognition, spectral analysis.

I. INTRODUCTION

RADAR target recognition is a very difficult task since the radar cross-section (RCS) of a target is highly dependent on operating frequency and aspect angle. To solve this problem, it is essential to obtain efficient and robust features from the RCS of a target, and therefore, range profiles, inverse synthetic aperture radar (ISAR) images, natural frequencies, and time-frequency signatures have been used for this purpose.

Range profiles of complex radar targets are the most easily obtainable feature vectors of the conventional radars. The range profile shows the RCS distribution of a target along the radial distance, which can provide information on the position and scattering strength of the target's scattering centers at that aspect [1]. One difficult problem with the range profile for use in target recognition is that it is highly aspect-dependent, and a large amount of data storage is required to provide adequate target recognition performance. Another problem is that its resolution has a significant effect on the final recognition results, and the range profiles of low resolution cannot provide robust and reliable feature vectors for target recognition. ISAR im-

ages show two-dimensional (2-D) RCS distribution of a target in the down-range and cross-range domain [2]. Although they can provide information about the 2-D position and strength of the scattering centers on the target, a sophisticated motion compensation algorithm to compensate for the translational and rotational motion of a moving target is needed to generate reliable ISAR images [3]. In addition, a huge amount of memory space is necessary to store the ISAR images for many aspects and target classes. Therefore, ISAR images may not be suitable for real-time target recognition due to their computational complexity.

Natural frequencies extracted from the late time responses of a target are aspect-independent, resulting in efficient feature vectors for target recognition [4]–[6]. However, for conventional high-frequency operating radars, the energy of the resonance contained in the late time portion of a signal is too small and is easily corrupted by noise. This is because no significant natural frequencies are excited in terms of the target's size and given high-frequency band. Therefore, it may be impossible to extract accurate natural frequencies of a target in a real situation. Recently introduced time-frequency signatures have some advantages over the range profiles or natural frequencies: they are able to show both early time responses such as scattering centers and late time responses such as resonance in a time-frequency plane [7]–[9]. However, they have a prohibitive memory space problem as in ISAR images, and resonance responses may not be identified in the time-frequency plane for the same reason as in natural frequencies.

Here, we consider range profiles as feature vectors for target recognition. Li and Yang [1] have developed a strategy based on range profile and used matching scores as a decision rule that utilizes normalized correlation coefficients. According to their algorithm, the matching score is defined as the maximum value of the correlation coefficients for all linear translational shifts between two range profiles. Therefore, their computational complexity grows rapidly as the number of target classes and aspect angles increases, unless accurate information about the target's aspect is available. Moreover, the enhancement of range resolution for the improvement of recognition accuracy increases the number of translation shifts to obtain a matching score between two range profiles, resulting in an additional computational cost. In view of target recognition, the matching score is robust against amplitude variations in the range profiles, but it is dominated by the strongest peak, which does not always originate from the same target. In addition to the above technique by Li and Yang, other correlation-based techniques have been proposed to compress the database for target recognition [10], [11].

Manuscript received May 23, 2001. This work was supported by the Korean Agency for Defense Development under Contract EM-44 and by the Ministry of Education of Korea under the BK 21 program.

K.-T. Kim is with the Department of Electrical Engineering and Computer Science, Yeungnam University, Kyongsan, Kyongbuk, 712-749, Korea.

D.-K. Seo is with the Graduate School for Information Technology, Pohang University of Science and Technology, Pohang, Kyungpook 790-784, Republic of Korea (e-mail: sdk@postech.ac.kr).

H.-T. Kim is with the Electrical and Computer Engineering Division, Pohang University of Science and Technology, Pohang, Kyungpook 790-784, Republic of Korea (e-mail: htkim@postech.ac.kr).

Publisher Item Identifier S 0018-926X(02)02623-6.

Zyweck and Bogner [12] used the magnitude of the Fourier transform of the preprocessed range profile to provide translation-invariant feature vectors. The feature vector based on this technique is the same regardless of the location of the target in the range window, so translational shifts, as in the case of matching scores, are not necessary. However, its dimension is still very large for high-resolution range profiles, and a large amount of storage is required to guarantee successful classification performance.

In this paper, we propose a recognition scheme based on the superresolution range profiles of the Multiple Signal Classification (MUSIC) algorithm and central moment features, which guarantee the translational invariance. Note that nearly all methodologies for target recognition discussed earlier are based on the range profiles obtained by conventional inverse fast Fourier transform (IFFT). Of course, much research has focused on the improvement of range resolution through superresolution techniques such as MUSIC [13], maximum likelihood [14], maximum entropy method [15], and Prony [16], but studies about their application to target recognition are rare. After the super-resolved range profiles are produced using the MUSIC algorithm, each range profile is normalized to its maximum amplitude in order to guarantee amplitude level (scattering strength) invariance. Next, central moment features of normalized range profiles are computed to provide translational invariance. Therefore, the central moment feature vectors of the normalized range profile have both the translation and level invariance, and hence they are dependent not on the position or overall amplitude level of the target response but only on its shape. Next, they are transformed into values between zero and unity to have the same “weight” in the Euclidean feature space. Next, the principal component analysis (PCA) is applied in order to eliminate their redundancy, resulting in feature vectors of a much smaller dimension. The resulting small dimensional features are combined with the Bayes classifier, based on the statistics of the data set. Experimental results using five aircraft models measured at the Pohang University of Science and Technology (POSTECH) compact range facility are presented to demonstrate the performance of the proposed technique. These results are compared with those of the range profiles obtained by IFFT.

II. PROPOSED SCHEME

A. Superresolved Range Profiles Using the MUSIC Algorithm

It was noted that a radar with higher range resolution can provide not only better recognition performance but also better tolerance to aspect variation, yielding significant advantage in saving memory space for establishing the database [17]. Therefore, it is crucial to enhance the range resolution for an efficient target recognition system. In a practical situation, however, the frequency bandwidth of a radar system is often limited by several factors, and the range profiles obtained by IFFT often result in a limited range resolution. In contrast, it is well known that the MUSIC algorithm provides superresolved range profiles of a target compared with those of the conventional IFFT for the same frequency bandwidth [13], [18]. Of course, the computational complexity of the MUSIC algorithm is much larger than

IFFT, but recently, the MUSIC processing can be completed within a real time due to the emergence of high-speed processors.

In the high-frequency region, the electric field backscattered from a complex radar target can be modeled approximately by a sum of fields scattered from some dominant scattering centers on the target. Therefore, the measured high-frequency RCS y_i at frequency f_i can be represented using undamped exponentials as

$$y_i = \sum_{k=1}^L a_k \exp\left(-j\frac{4\pi f_i}{c} r_k\right) + n_i, \quad i = 1, 2, \dots, N \quad (1)$$

where r_k is the location of the k th scattering center, a_k is the associated amplitude, L is the number of scattering centers on the target, n_i is the measurement noise, N is the number of frequency measurements, and c is the speed of light.

Rewriting (1) in vector notation, it can be expressed as

$$\mathbf{y} = \mathbf{E}\mathbf{a} + \mathbf{n} \quad (2)$$

where

$$\begin{aligned} \mathbf{y} &= [y_1, y_2, \dots, y_N]^T \\ \mathbf{E} &= [\mathbf{e}(r_1), \mathbf{e}(r_2), \dots, \mathbf{e}(r_L)] \\ \mathbf{e}(r_k) &= \left[\exp\left(-j\frac{4\pi f_1}{c} r_k\right), \exp\left(-j\frac{4\pi f_2}{c} r_k\right), \dots, \right. \\ &\quad \left. \exp\left(-j\frac{4\pi f_N}{c} r_k\right) \right]^T \\ \mathbf{a} &= [a_1, a_2, \dots, a_L]^T \\ \mathbf{n} &= [n_1, n_2, \dots, n_N]^T. \end{aligned}$$

In the above, \mathbf{y} is an $N \times 1$ data vector, \mathbf{E} is an $N \times L$ matrix, $\mathbf{e}(r_k)$ is a direction vector of length N , \mathbf{a} is an $L \times 1$ amplitude vector, and \mathbf{n} is an $N \times 1$ noise vector.

To obtain superresolution range profiles using the MUSIC algorithm, the covariance matrix \mathbf{R}_{yy} of the received signal \mathbf{y} should be estimated. If the noises n_i are assumed to be uncorrelated and to have identical variance σ^2 , the covariance matrix \mathbf{R}_{yy} is defined as

$$\mathbf{R}_{yy} = E[\mathbf{y}\mathbf{y}^H] = \mathbf{E}\mathbf{A}\mathbf{A}^H + \sigma^2\mathbf{I} \quad (3)$$

where $\mathbf{A} = E[\mathbf{a}\mathbf{a}^H]$, \mathbf{I} is the identity matrix and H denotes complex conjugate transpose. Because the exact covariance matrix \mathbf{R}_{yy} in (3) is an average over a number of snapshots but only one snapshot is available in radar applications, a special technique known as spatial smoothing preprocessing (SSP) may be used to estimate \mathbf{R}_{yy} [19]. However, modified spatial smoothing preprocessing (MSSP) has been shown to exhibit an improved performance over SSP in decorrelating signals from various scattering centers [18].

Applying the MSSP, the covariance matrix can be estimated as follows:

$$\hat{\mathbf{R}}_{yy} = \frac{1}{2M} \sum_{k=1}^M (\mathbf{R}_k + \mathbf{J}\mathbf{R}_k^*\mathbf{J}) \quad (4)$$

where

$$\begin{aligned}\mathbf{R}_k &= \mathbf{y}_k \mathbf{y}_k^H \\ \mathbf{y}_k &= [y_k, y_{k+1}, \dots, y_{k+m-1}]^T \\ \mathbf{J} &= \begin{bmatrix} 0 & \cdots & 0 & 1 \\ 0 & \cdots & 1 & 0 \\ \vdots & & \vdots & \vdots \\ 1 & 0 & \cdots & 0 \end{bmatrix}.\end{aligned}$$

In (4), M is the number of subarrays, m is the subarray dimension, \mathbf{J} is the $m \times m$ exchange matrix, and $*$ denotes complex conjugate. \mathbf{y}_k is the data vector of the k th subarray of size m , as shown in Fig. 1.

It should be noted that, as shown in Fig. 1 and (4), the resolution of the MSSP is reduced, since the effective bandwidth decreases from N to m . In spite of this disadvantage, the MUSIC algorithm combined with the MSSP gives a much better performance than the conventional IFFT [18]. In the MSSP, the decorrelation effect is obtained at the expense of a reduced effective bandwidth. If m increases, the resolution of the MUSIC algorithm improves, but the decorrelation performance between signals from different scattering centers is degraded. In contrast, as m decreases, the decorrelation performance improves, whereas the resolution is degraded. Therefore, in terms of target recognition, there are some tradeoffs in choosing m . That is, if m is large, the MUSIC algorithm can provide range profiles of high resolution but some dominant scattering centers may not be detected due to the degradation of the decorrelation performance, and vice versa.

Using the MUSIC algorithm, we can estimate the superresolved range profile of a target as

$$p_m(r) = \frac{1}{\sum_{i=L+1}^m |\mathbf{u}_i^H \mathbf{e}(r)|^2} \quad (5)$$

where \mathbf{u}_i is the eigenvectors corresponding to the minimum (noise) eigenvalues of $\hat{\mathbf{R}}_{yy}$. Note that the MUSIC algorithm takes advantage of the fact that the direction vector $\mathbf{e}(r_k)$ is orthogonal to the noise subspace consisting of $(m - L)$ noise eigenvectors $\mathbf{u}_{L+1}, \mathbf{u}_{L+2}, \dots, \mathbf{u}_m$.

In (5), the selection of L plays an important role in the stable operation of the MUSIC algorithm. If the estimated \hat{L} is less than true L , $p_m(r)$ may miss some dominant scattering centers on the target, whereas if it is greater than L , spurious peaks might appear. For an accurate estimation of \hat{L} , the information-based criteria such as Akaike information criterion and minimum description length can be used [20], [21], but they are computationally intensive and furthermore they often fail to predict accurate values of \hat{L} for noise-corrupted signals. On the other hand, from empirical studies in [18], a sharp spurious peak did not appear even when the estimated \hat{L} is larger than L since an orthogonality relationship between the direction vector $\mathbf{e}(r_k)$ and $(m - \hat{L})$ noise eigenvectors still holds when \hat{L} is larger than L .

B. Feature Extraction Based on Central Moments

Moments and functions of moments have been utilized as pattern features in a number of applications to achieve invariant

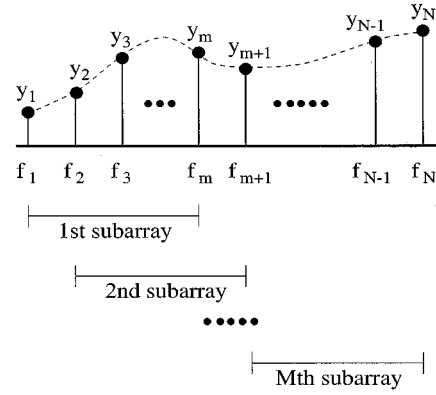


Fig. 1. Subarray configuration for the MSSP.

recognition of 2-D image patterns [22]–[26]. To guarantee the translation, scale, contrast, and rotation invariance, various moments such as Hu moment invariants, Zernike moments, Legendre moments, and complex moments have been used in the 2-D pattern recognition community [27]. However, in this study, we only need translational and scale (level) invariance to classify one-dimensional (1-D) image (i.e., range profile) patterns. In 1-D pattern recognition, the level invariance can be accomplished through an appropriate preprocessing proposed in this paper, and the simple central moments satisfy the translational invariance [22].

For a fixed bandwidth and polarization, the range profile of a target measured by the radar depends on the distance and aspect between the radar and target. That is, for a fixed aspect, the returned signal from the target decays as it travels, and its range profile from a far-away target has the target responses with low amplitude levels, and vice versa. However, in general, the overall shape of the target response of a specific target does not change with the distance when the aspect is fixed, and absolute amplitude of target response has no significant meaning. Therefore, in order to construct the database for target recognition, we need only to store the shapes of the range profiles as a function of aspect rather than as a function of distance, resulting in significant savings of computational resources. To meet this requirement, the range profile of a target at each aspect is normalized to its value of maximum peak (strongest scattering center), and therefore the range profile does not depend on the distance but only on the aspect. Furthermore, this normalization reduces the aspect dependence or weight of the signal levels of the target's responses. The overall amplitude levels of the range profiles within the same target fluctuate with the aspect, and its levels at certain aspects may be much higher than those at other aspects. This may cause a significant difference between the two range profiles of a target at two different aspects even though their relative shapes are similar, yielding unwanted bias or weight in the feature space domain. Using the above normalization, two similar-shaped range profiles of a target at two different aspects guarantee their closeness in the Euclidean feature space even though their overall amplitude levels are quite different. Hence, for each target class, the features at various aspect angles are well grouped together to form a cluster in the feature space domain. As a result, the desired level invariance has been achieved

through this preprocessing, and the discrimination between different target classes can be performed only by the shapes of normalized range profiles, not by their signal levels.

The p th order central moments μ_p of a function $f(x)$ are defined as

$$\mu_p = \int_{-\infty}^{\infty} (x - \eta_x)^p f(x) dx \quad (6)$$

where

$$\begin{aligned} \eta_x &= \int_{-\infty}^{\infty} x f(x) dx \\ 1 &= \int_{-\infty}^{\infty} f(x) dx. \end{aligned}$$

The central moments μ_p are projections onto $(x - \eta_x)^p$ so that they become invariant under translation, but note that they have substantial redundancy since the monomials $(x - \eta_x)^p$ are not orthogonal. In [27], the information redundancy of the geometric moments, which is equivalent to that of the central moments, was analyzed to show the ratio between the informative part and redundant part as a function of moment order p . According to the results, the ratio decays exponentially as p increases, and this implies that the information contained in the high-order central moments is already provided in the lower order central moments. This problem can be circumvented by the use of orthogonal moments such as Zernike or Legendre moments, which are based on the theory of orthogonal polynomials. However, in the presence of noise, the geometric moments, i.e., the central moments, are more robust than the Zernike and Legendre moments [27]. Because the range profiles of a target are often corrupted by noise, the central moments may provide more stable features for target recognition than other orthogonal moments. Furthermore, the redundancy contained in the central moments can be effectively eliminated by the principal component analysis (PCA), to be discussed later.

After the preprocessing and discrete sampling of the range profile in (5), its p th order central moment can be computed by

$$\mu_p = \sum_{i=1}^{N_r} (r_i - \eta_r)^p \left[\frac{\bar{p}_m(r_i)}{\sum_{i=1}^{N_r} \bar{p}_m(r_i)} \right], \quad r_i \in [0, R_u] \quad (7)$$

where

$$\eta_r = \sum_{i=1}^{N_r} r_i \left[\frac{\bar{p}_m(r_i)}{\sum_{i=1}^{N_r} \bar{p}_m(r_i)} \right]$$

where $\bar{p}_m(r_i)$ is the normalized range profile after the preprocessing, N_r is the number of range bin sampling, and R_u is the maximum unambiguous range.

Note that the noise terms outside of the target response in the range profile may have an effect on the final value of the central moments μ_p in (7). As the noise power contained in the received signal increases, spurious peaks due to noises appear in the range profile $\bar{p}_m(r_i)$. In general, since the target response is concentrated on a limited region of r_i in the range profile, the remaining part of the range profile excluding the target response is often corrupted by noise, resulting in many spurious peaks. Therefore, the central moments from the noise-corrupted

range profile may be more unstable as the number of range bin sampling N_r increases, though the noise power contained in the received signal is negligibly small. This problem can be mitigated using the range window around the target response. Because the distance information from the radar to the target is available in any conventional radar, we select only the range profile around the target response, and the $\bar{p}_m(r_i)$ s outside of the target response are set to zeros.

We also note that the magnitude of moments may grow exponentially with increasing order p . This problem may cause the central moments with higher orders to be more sensitive to noise or quantization error, resulting in unstable features, and can be mitigated by mapping the range values r_i into $[0, 1]$ rather than $[0, R_u]$. This mapping can be achieved by choosing the resolution of range bin sampling as $\Delta r = (1/(N_r - 1))$, yielding $|r_i - \eta_r| < 1$. Therefore, the magnitude of central moments decays exponentially with increasing order p , and it may be less sensitive to noise or quantization error.

Using the central moments in (7), the feature vector \mathbf{f} can be represented as

$$\begin{aligned} \mathbf{f} &= [f_1, f_2, \dots, f_{p_{\max}}]^T \\ &= [\mu_1, \mu_2, \dots, \mu_{p_{\max}}]^T \end{aligned} \quad (8)$$

where p_{\max} is the maximum order of central moments used to form a feature vector. The selection of p_{\max} is dependent on the specific problem at hand. Note that there is no absolutely right way of choosing optimum p_{\max} . For the feature extraction from a complex 2-D image, it is necessary to compute the moments up to high orders since high-frequency spectral contents such as edges and corners cannot be described only with low-order moments. However, the computational cost increases with an increase in p_{\max} , but a too large value of p_{\max} does not improve classification accuracy. For example, seven different moment invariants derived by Hu [22] are composed of central moments only from zeroth to third order, which were successfully applied to classify 2-D image patterns. For representing a 1-D range profile in this study, we think that a too large value of p_{\max} may add a computational burden without improving recognition accuracy because the central moments have more information redundancy as the order p increases. Furthermore, the higher order moments are more sensitive to additive white Gaussian noise (AWGN) [27]. From several experiments in this study, we found that $p_{\max} = 20$ is sufficient for classifying 1-D range profiles from different targets, but a smaller value may be enough to guarantee the classification accuracy for range profiles with smaller amplitude variations.

To design a classifier, it is necessary to construct a training database containing feature vectors of many target classes and aspect angles. For N_c target classes and N_a aspects used for training, we can obtain the training database \mathbf{F} using (8) as follows:

$$\mathbf{F} = \begin{bmatrix} f_{11} & f_{12} & \cdots & f_{1Q} \\ f_{21} & f_{22} & \cdots & f_{2Q} \\ \vdots & \vdots & & \vdots \\ f_{p_{\max},1} & f_{p_{\max},2} & \cdots & f_{p_{\max},Q} \end{bmatrix} \quad (9)$$

where $Q = N_c \times N_a$ and \mathbf{F} is a $p_{\max} \times Q$ matrix.

Because the magnitudes of central moments obtained in (8) decrease rapidly as the order increases, the magnitude of element f_{ij} in \mathbf{F} also decreases rapidly as i increases for any fixed j . However, the obtained central moments should have the same “weight” in the Euclidean feature space irrespective of orders p for improving classification accuracy. Therefore, we transform the elements of \mathbf{F} into values between zero and unity to provide equal weight in each dimension of the feature space as follows:

$$\bar{f}_{ij} = \frac{f_{ij} - f_{i,\min}}{f_{i,\max} - f_{i,\min}}, \quad i = 1, 2, \dots, p_{\max}, \quad j = 1, 2, \dots, Q \quad (10)$$

where

$$\begin{aligned} f_{i,\min} &= \text{minimum } f_{ij}, \quad j = 1, 2, \dots, Q \quad \text{for a given } i \\ f_{i,\max} &= \text{maximum } f_{ij}, \quad j = 1, 2, \dots, Q \quad \text{for a given } i \end{aligned}$$

and therefore the normalized training database $\bar{\mathbf{F}}$ is established as follows:

$$\bar{\mathbf{F}} = \begin{bmatrix} \bar{f}_{11} & \bar{f}_{12} & \cdots & \bar{f}_{1Q} \\ \bar{f}_{21} & \bar{f}_{22} & \cdots & \bar{f}_{2Q} \\ \vdots & \vdots & & \vdots \\ \bar{f}_{p_{\max},1} & \bar{f}_{p_{\max},2} & \cdots & \bar{f}_{p_{\max},Q} \end{bmatrix}. \quad (11)$$

Note that any test data for demonstrating the performance of the proposed technique in this paper will also be normalized using (10) from the training database.

C. Redundancy Reduction Using Principal Component Analysis

As discussed earlier, the central moment features show more redundant information as the order p increases. The redundancy contained in the feature vectors often adds the computational cost to the classifier stage without increasing recognition accuracy. To deal with this difficulty, the PCA is applied to the normalized training database $\bar{\mathbf{F}}$. With the PCA, the redundancy contained in the features can be effectively reduced, and furthermore the dimensionality reduction can be achieved [28]. That is, the transformation based on the PCA is designed in such a way that the data set may be represented by a reduced number of “effective” features and yet retain most of the intrinsic information content of the data.

Let $\bar{\mathbf{f}}_k$ be the k th column vector of the normalized training data matrix $\bar{\mathbf{F}}$ in (11)

$$\bar{\mathbf{F}} = [\bar{\mathbf{f}}_1, \bar{\mathbf{f}}_2, \dots, \bar{\mathbf{f}}_Q]. \quad (12)$$

Next, the sample mean vector $\mathbf{m}_{\bar{\mathbf{F}}}$ and the sample covariance matrix $\mathbf{R}_{\bar{\mathbf{F}}\bar{\mathbf{F}}}$ can be obtained by

$$\mathbf{m}_{\bar{\mathbf{F}}} = \frac{1}{Q} \sum_{k=1}^Q \bar{\mathbf{f}}_k \quad (13)$$

$$\mathbf{R}_{\bar{\mathbf{F}}\bar{\mathbf{F}}} = \frac{1}{Q-1} \sum_{k=1}^Q (\bar{\mathbf{f}}_k - \mathbf{m}_{\bar{\mathbf{F}}})(\bar{\mathbf{f}}_k - \mathbf{m}_{\bar{\mathbf{F}}})^T \quad (14)$$

where $\mathbf{m}_{\bar{\mathbf{F}}}$ is a $p_{\max} \times 1$ vector and $\mathbf{R}_{\bar{\mathbf{F}}\bar{\mathbf{F}}}$ is a $p_{\max} \times p_{\max}$ matrix.

Let the eigenvalues of $\mathbf{R}_{\bar{\mathbf{F}}\bar{\mathbf{F}}}$ be denoted by $\lambda_1, \lambda_2, \dots, \lambda_{p_{\max}} (\lambda_1 > \lambda_2 > \dots > \lambda_{p_{\max}})$ and the associated

eigenvectors be denoted by $\mathbf{v}_1, \mathbf{v}_2, \dots, \mathbf{v}_{p_{\max}}$. Then, the sample covariance matrix $\mathbf{R}_{\bar{\mathbf{F}}\bar{\mathbf{F}}}$ can be decomposed as follows:

$$\mathbf{R}_{\bar{\mathbf{F}}\bar{\mathbf{F}}} = \mathbf{V} \Lambda \mathbf{V}^T \quad (15)$$

where

$$\begin{aligned} \Lambda &= \text{diag}[\lambda_1, \lambda_2, \dots, \lambda_{p_{\max}}] \\ \mathbf{V} &= [\mathbf{v}_1, \mathbf{v}_2, \dots, \mathbf{v}_{p_{\max}}]. \end{aligned}$$

Then, the transformation matrix \mathbf{P} can be constructed using \mathbf{V} and is given by

$$\mathbf{P} = [\mathbf{v}_1, \mathbf{v}_2, \dots, \mathbf{v}_l] \quad (16)$$

where $l < p_{\max}$ and $\mathbf{v}_1, \mathbf{v}_2, \dots, \mathbf{v}_l$ are the eigenvectors corresponding to the largest l eigenvalues. The remaining $(p_{\max} - l)$ eigenvalues are negligibly small. Each feature vector of dimension p_{\max} from both the training data set and the test data set can be transformed into a new feature space of dimension l as follows:

$$\mathbf{x}_k = \mathbf{P}^T \bar{\mathbf{f}}_k. \quad (17)$$

Note that the sample mean and sample covariance matrix are computed from the training data set only, and the same transform matrix is used for redundancy elimination in both training and test samples.

After the PCA, variances of high-order components of a new feature vector \mathbf{x}_k are near zero since redundancy in the original feature space is removed. Therefore, high-order components in the new feature vector can be ignored, and the original feature space can be reduced to a new feature space whose dimension is smaller than p_{\max} .

The compression ratio p_{\max}/l is dependent on how much redundant information is contained in the feature vectors. In this study, the redundant information may increase as the maximum order p_{\max} used to form a feature vector in (8) increases because higher order central moments have more redundancy. Therefore, the value of l does not increase if p_{\max} is larger than a certain threshold because the number of largest eigenvalues of $\mathbf{R}_{\bar{\mathbf{F}}\bar{\mathbf{F}}}$ no longer increases. We found that $p_{\max} = 20$ is the typical threshold for the range profiles of the five targets used in this study.

D. Bayes Classifier

We have now final training feature vectors $\mathbf{x}_k, k = 1, 2, \dots, Q$ to design a classifier to classify a test feature vector \mathbf{x}_u whose class is unknown. In this paper, one of the well-known statistical methods, Bayes classifier, is selected to perform classification of \mathbf{x}_u .

The Bayes classifier is optimum in the sense of probability of error, and it is a parametric procedure [29]. Therefore, it requires the joint probability density function of the feature of each class as well as the *a priori* probability of each class. However, such information is not available in general, and it should be estimated from the training feature vectors. Usually, the distribution of the training data set is assumed to be a multivariate normal, and a priori probability of each class is the same. We take the above assumption for simplicity since the preprocessing

and feature extraction techniques mentioned in the previous sections may provide the feature vectors to be well clustered across the aspects. Hence the assumption of the multivariate normal distribution may be valid.

Supposing that the training features have a multivariate normal distribution and equal class probability, the Bayes rule determines the class of test feature vector \mathbf{x}_u as

$$\hat{i} = \max_i g_i(\mathbf{x}_u) \quad (18)$$

with

$$g_i(\mathbf{x}_u) = -\frac{1}{2} \log |\mathbf{C}_i| - \frac{1}{2} (\mathbf{x}_u - \mathbf{m}_i)^T \mathbf{C}_i^{-1} (\mathbf{x}_u - \mathbf{m}_i) \quad (19)$$

where \mathbf{m}_i and \mathbf{C}_i are the sample mean vector and sample covariance matrix of class i , respectively, and \hat{i} varies from one to N_c since we have N_c target classes.

III. ALGORITHM SUMMARY

So far, the proposed scheme for target recognition has been discussed in detail, and it is summarized as follows.

- 1) For N_c target classes and N_a aspects used for training, compute range profiles using the MUSIC spectrum estimator in (5).
- 2) Normalize each range profile using its maximum peak.
- 3) Apply the range window to the normalized range profile $\bar{p}_m(r_i)$.
- 4) Compute the central moments up to order p_{\max} using (7) but with $r_i \in [0, 1]$ where the resolution of range bin sampling is equal to $\Delta r = (1/(N_r - 1))$.
- 5) Construct the training database \mathbf{F} .
- 6) Map each element of \mathbf{F} into values between zero and unity using (10), resulting in $\bar{\mathbf{F}}$.
- 7) Apply the PCA to the column vectors of $\bar{\mathbf{F}}$ to obtain the transformation matrix \mathbf{P} .
- 8) With the use of \mathbf{P} , transform the column vectors of $\bar{\mathbf{F}}$ into \mathbf{x}_k , $k = 1, 2, \dots, Q$, where $Q = N_c N_a$.
- 9) Design a Bayes classifier in (18) and (19) using the obtained training feature vectors \mathbf{x}_k , $k = 1, 2, \dots, Q$.
- 10) For any target and aspect used for testing, perform Steps 1)–4), 6), and 8) to obtain the test feature vector \mathbf{x}_u whose class is unknown, and identify its class using the designed Bayes classifier in Step 9).

Note that the transformations of feature vectors in Steps 6) and 8) are based on the training data samples only, and the same transformations are applied to both the training and test feature vectors. In the proposed procedures described above, Step 1) can be replaced with range profiles from other superresolution spectrum estimators or IFFT.

The computational bottleneck of the training phase occurs in Steps 1) and 7) because they need computationally intensive eigendecomposition, and the major computational cost in the testing phase comes from Step 1) only. In Step 1), the dimension of the covariance matrix $\hat{\mathbf{R}}_{yy}$ is $m \times m$, where m is a subarray dimension that we select, and the MUSIC algorithm requires the eigendecomposition of $\hat{\mathbf{R}}_{yy}$. Therefore, the selection of subarray dimension m is most important in reducing the computation time for both the training phase and the testing phase.

As m decreases, the computation time may be reduced, but the resolution is degraded, and vice versa. For computational efficiency, IFFT can be used in Step 1) instead of MUSIC. However, the MUSIC algorithm can provide range profiles of much higher resolution than those of the IFFT, and therefore the proposed technique can ensure the successful correct classification rate even for a relatively small value of m , as will be shown in the next section.

IV. EXPERIMENTAL RESULTS

To demonstrate the proposed technique, we chose five different aircraft models shown in Fig. 2. Their physical sizes are about 1 m, and their RCS were measured at the POSTECH compact range facility. The frequency bandwidth of the measurements ranges from 8.3 to 12.3 GHz (X-band) with a 0.01-GHz increment, yielding 401 frequency samples, and aspect angles in the azimuth plane ranges from 30.2° to 59.8° with respect to the target's head using a 0.4° step, resulting in 75 aspects for each target. The elevation angle of each target is fixed at 0° . Both the horizontally transmitting–horizontally receiving (HH) and vertically transmitting–vertically receiving (VV) polarizations were used for the measurements.

Note that the size of each target at a frequency of 10 GHz is merely about 33 wavelengths, and therefore some small substructures on each target may be in the resonance region rather than in the high-frequency region. On the other hand, the size of an actual aircraft whose physical size is 30 m corresponds to 1000 wavelengths at 10 GHz, and its substructures are strictly in the high-frequency region. In addition, the range resolution of the measured 4-GHz bandwidth is 3.75 cm, and the response of a target with 1 m dimension is represented only about 27 Fourier bins in the range profile domain. However, an actual target of 30 m dimension corresponds to 800 Fourier bins for the same bandwidth. Therefore, the experimental setup in this study is a very difficult condition for target recognition compared to that of a real situation consisting of an actual-sized target under an X-band operating radar.

Fig. 3 shows the RCS values for the five targets measured at the POSTECH compact range. It is clearly observed from this figure that the RCS of each target is highly dependent on its aspect angle. For example, Fig. 3(a) and (c) shows that the RCS around the angle 35° is much larger than other aspect regions. Furthermore, as previously mentioned, resonant-like scattering at 9 and 12.3 GHz, which is independent of aspect angle, is seen in Fig. 3(d). Note that the absolute RCS levels of the five targets are all different, and Target 4 has much lower RCS values than the others. Therefore, the absolute amplitude levels of the range profiles for the five targets are different, but the proposed technique in this paper uses their shapes only irrespective of their levels. Using the RCS data at an aspect of 30.2° in Fig. 3, the normalized range profiles of the MUSIC algorithm and IFFT for the five targets are shown in Fig. 4.

Before target recognition experiments, the data sets must be divided into a training set and a test set. We have five target classes, and the data set from each target includes 75 aspects. So $5 \times 75 = 375$

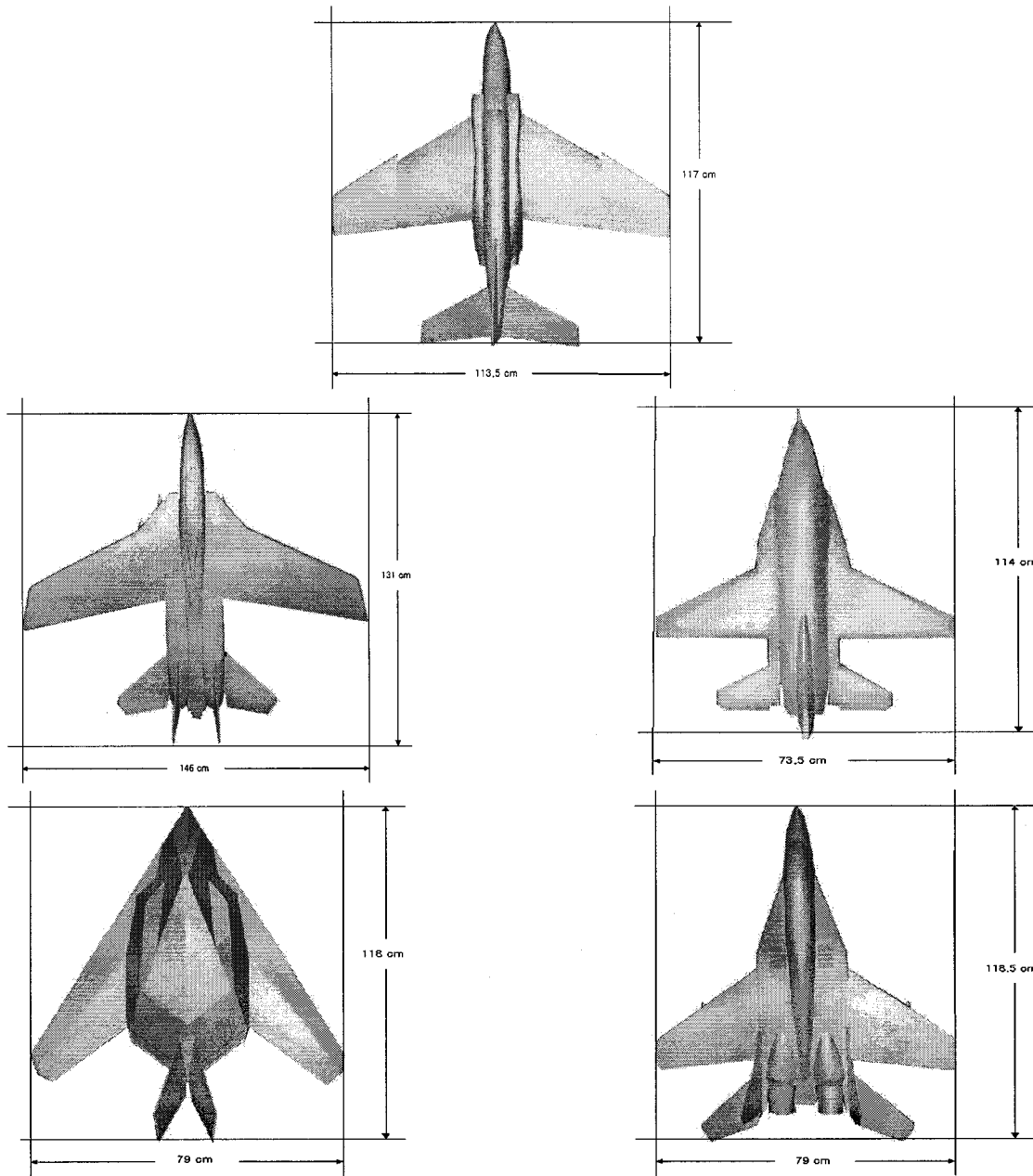


Fig. 2. Five aircraft models to demonstrate the proposed technique.

data sets must be subdivided with respect to their aspects to form a training set and a test set. Assume the training data set comes from uniform angle sampling with an increment of 1.6° , corresponding to 19 aspects for each target. Therefore, we have 5 (number of target classes) \times 19 (number of aspects for training) $= 95$ data sets for constructing the training database, and the remaining $(375 - 95) = 280$ data sets are reserved for testing. Hence the training set size is only $95/375 = 25.33\%$ of the overall data set, resulting in 74.67% for testing. Table I shows the sizes of training sets and test sets for three different angle increments used for training in this study. The experimental results to be demonstrated later are based on one of the three data sets in Table I.

A. Effect of Subarray Dimension

As discussed earlier, the selection of the subarray dimension m is crucial to the stable operation of the MUSIC algorithm and therefore to successful target recognition. Since the MSSP is used to estimate the covariance matrix $\hat{\mathbf{R}}_{yy}$, one can successfully apply the MUSIC algorithm to this smoothed covariance matrix regardless of the coherence of the signals. However, this robustness comes at the expense of a reduced effective bandwidth. The number of subarrays M is given by $M = N - m + 1$, where N is the number of frequency samples. Because N is fixed in general, the increase of m reduces the number of subarrays M , and therefore the decorrelation performance of MSSP is degraded. Further, the decrease of m reduces the effective bandwidth, degrading the resolution of the MUSIC estimator.

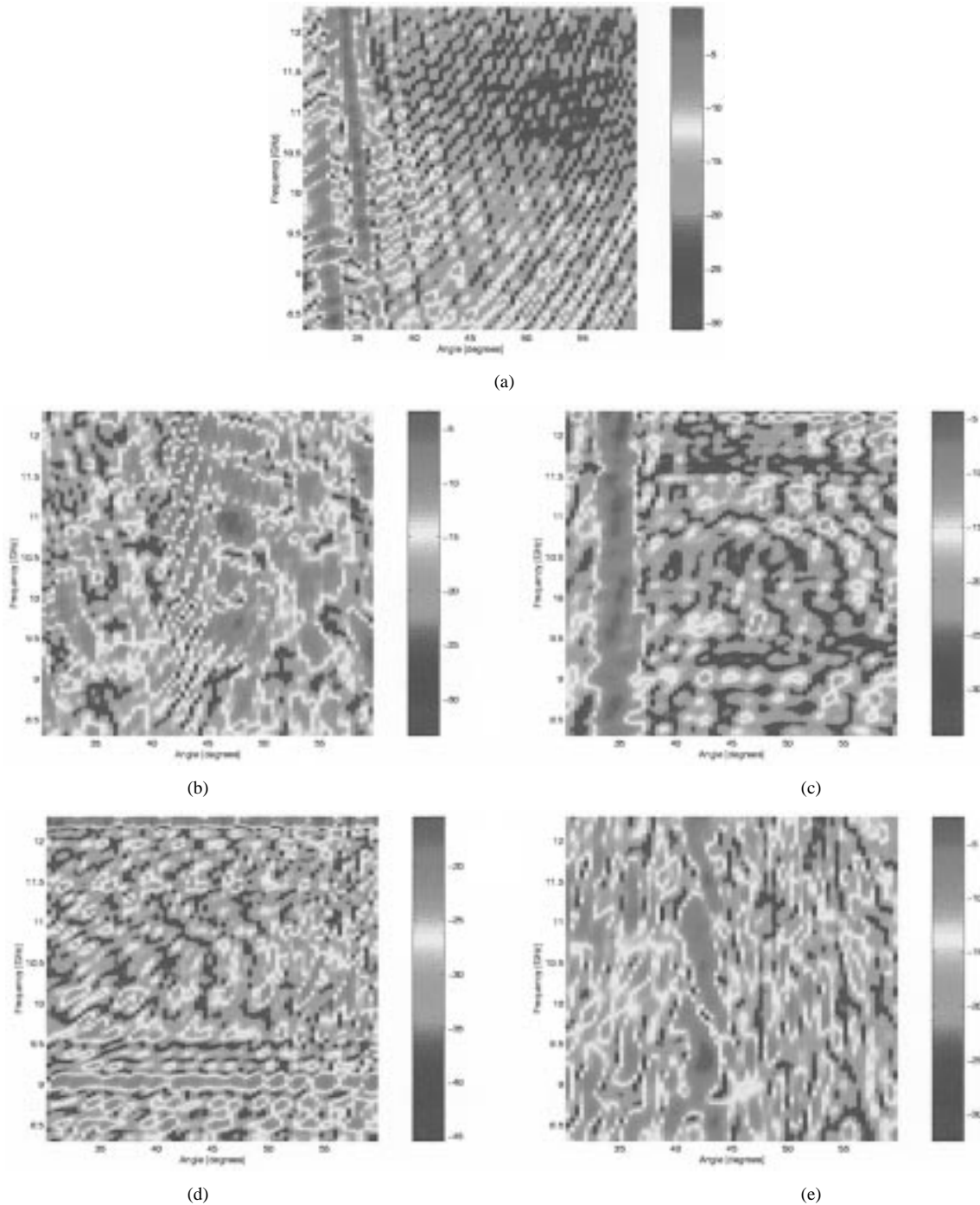


Fig. 3. Angle versus frequency display of the RCS for the five targets at the fixed elevation angle 0° : frequency bandwidth = 8.3–12.3 GHz with a frequency step of 0.01 GHz, azimuth angle region = 30.2° – 59.8° with an angle step of 0.4° , and HH polarization. The color levels represent RCS values in dB. (a) Target 1, (b) Target 2, (c) Target 3, (d) Target 4, and (e) Target 5.

On the other hand, the decorrelation performance is improved. For a target consisting of L scattering centers, the number of subarrays $M = N - m + 1$ must be greater than or equal to L in order to guarantee the successful decorrelation of L coherent signals, and also m must be at least $L+1$. Therefore, the minimum number of frequency sampling N is equal to $2L$ [18]. The subarray dimension m has been chosen such that the effective bandwidth is about half the available bandwidth, i.e., $m/N \approx 0.5$, to ensure the required resolution in ISAR images [30].

To investigate the performance of the proposed technique in terms of the subarray dimension m , we utilized SET-1 to estimate the correct recognition rate P_c , which is given by

$$P_c = \frac{\text{Number of correct classifications}}{\text{Number of test samples}}. \quad (20)$$

The polarization was chosen as HH, and $\hat{L} = 30$ was used for the MUSIC algorithm to estimate at least 30 scattering centers on the target. When the number of scattering centers on the

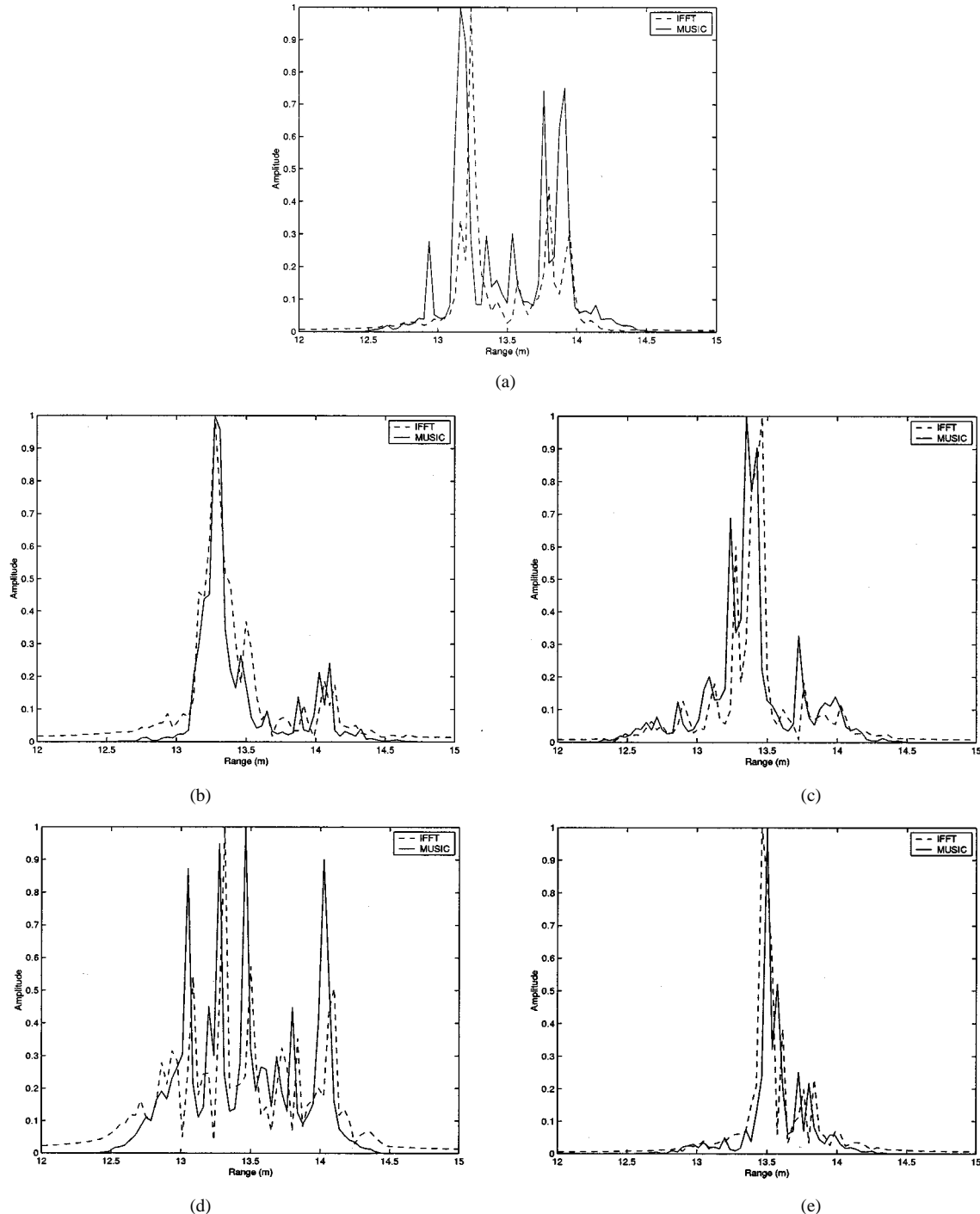


Fig. 4. Normalized range profiles obtained by MUSIC and IFFT: frequency bandwidth = 8.3–12.3 GHz, aspect angle = 30.2° , and HH polarization. The dashed lines come from the 401-point IFFT, and the solid lines come from the MUSIC algorithm with $m = 134$, $\hat{L} = 30$ and $N_r = 401$. (a) Target 1, (b) Target 2, (c) Target 3, (d) Target 4, and (e) Target 5.

target is less than 30, spurious peaks may appear, but the major portion of the spurious peaks can be effectively reduced by a range window of 3 m in length. $N_r = N$ was used to sample the range profile of the MUSIC algorithm, and $p_{\max} = 20$ was used to compute the central moments of the range profiles. After the PCA, the largest seven eigenvalues are kept to produce the transformation matrix \mathbf{P} , and therefore l , the dimension of the final feature vector, is seven. Note that in the case of $N_r = 401$, a large compression ratio of $(N_r/l) = (401/7) = 57.29$ can be achieved via the proposed algorithm based on central moments

and PCA. The results of P_c as a function of m/N are shown in Fig. 5.

In Fig. 5, the horizontal axis denotes the effective bandwidth m/N , and the vertical axis denotes the correct recognition rate P_c . We performed the experiments based on three different bandwidths, 2, 3, and 4 GHz, and the corresponding N s are $N = 201$, $N = 301$ and $N = 401$, respectively. In the case of the 2 GHz bandwidth, P_c slowly decreases when m/N is larger than the threshold 0.3. The respective threshold values of m/N for 3 and 4 GHz bandwidths are 0.4 and 0.5. For m/N

TABLE I
SUBDIVISION OF TRAINING AND TEST DATASETS (EQUIVALENT PERCENTAGES WITH RESPECT TO THE OVERALL DATA SIZE ARE GIVEN IN PARENTHESES)

Data Set	Angular Increment for Training	Training Set Size	Testing Set Size	Total Size
SET-1	0.8°	$5 \times 38 = 190$ (50.67%)	$5 \times 37 = 185$ (49.33%)	375 (100%)
SET-2	1.6°	$5 \times 19 = 95$ (25.33%)	$5 \times 56 = 280$ (74.67%)	375 (100%)
SET-3	3.2°	$5 \times 10 = 50$ (13.33%)	$5 \times 65 = 325$ (86.67%)	375 (100%)

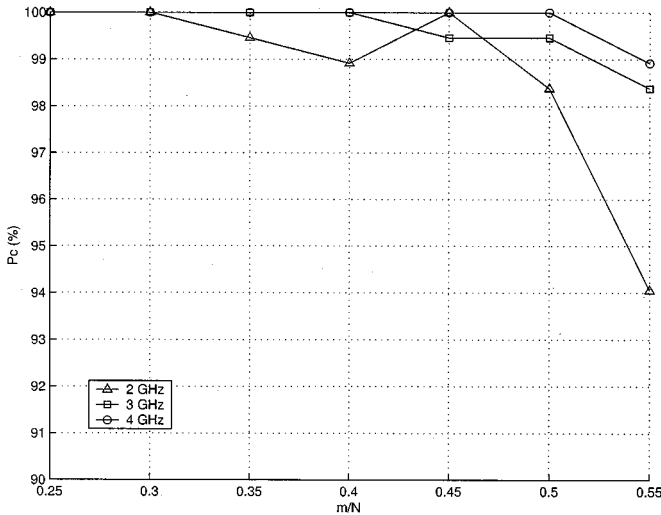


Fig. 5. P_c versus effective bandwidth m/N display using the SET-1 and HH polarization. The data with a 2 GHz bandwidth: 8.3–10.3 GHz, $N = N_r = 201$, $\hat{L} = 30$, $p_{\max} = 20$, and $l = 7$. The data with a 3 GHz bandwidth: 8.3–11.3 GHz, $N = N_r = 301$, $\hat{L} = 30$, $p_{\max} = 20$, and $l = 7$. The data with a 4 GHz bandwidth: 8.3–12.3 GHz, $N = N_r = 401$, $\hat{L} = 30$, $p_{\max} = 20$, and $l = 7$.

TABLE II
CONFUSION MATRIX OF THE MUSIC ALGORITHM USING SET 2 AND HH POLARIZATION. THE SELECTED PARAMETERS ARE: BANDWIDTH = 8.3–12.3 GHz, $N = N_r = 401$, $m = 134$, $\hat{L} = 30$, $p_{\max} = 20$, AND $l = 7$ (OVERALL CORRECT RECOGNITION RATE $P_c = 99.64\%$)

Actual Class	Classification				
	Target-1	Target-2	Target-3	Target-4	Target-5
Target-1	56	0	0	0	0
Target-2	0	56	0	0	0
Target-3	0	0	56	0	0
Target-4	1	0	0	55	0
Target-5	0	0	0	0	56

values smaller than each threshold, P_c reaches 100% irrespective of bandwidth. Note that P_c maintains 100% even for a relatively small m/N since the MUSIC algorithm can provide superresolved range profiles even for a small bandwidth. The decrease of P_c when m/N is larger than each threshold comes from the fact that M , the number of subarrays, decreases as m increases, and this degrades the decorrelation performance of the MSSP. Furthermore, as N (i.e., bandwidth) decreases, the threshold decreases due to the decrease in the available M for the same m . The computational complexity increases with

TABLE III
CONFUSION MATRIX OF THE MUSIC ALGORITHM USING SET 2 AND VV POLARIZATION. THE SELECTED PARAMETERS ARE: BANDWIDTH = 8.3–12.3 GHz, $N = N_r = 401$, $m = 134$, $\hat{L} = 30$, $p_{\max} = 20$ AND $l = 7$ (OVERALL CORRECT RECOGNITION RATE $P_c = 99.64\%$)

Actual Class	Classification				
	Target-1	Target-2	Target-3	Target-4	Target-5
Target-1	56	0	0	0	0
Target-2	0	56	0	0	0
Target-3	0	0	56	0	0
Target-4	0	0	1	55	0
Target-5	0	0	0	0	56

the increase of m since the eigendecomposition of $\hat{\mathbf{R}}_{yy}$ with the size of $m \times m$ is needed to compute the superresolved range profile of the MUSIC estimator. Considering the above three conflicting requirements of resolution, decorrelation, and computation time, we select the subarray dimension m such that $m/N \approx 1/3$, which will be used for all later experiments.

Tables II and III show the confusion matrices of the proposed scheme using SET 2 in Table I. The polarizations in Tables II and III are based on HH and VV, respectively, and the bandwidth of 4 GHz is used, resulting in $N = 401$. Therefore, we selected the subarray dimension as $m = 134$ in order to satisfy $m/N \approx 1/3$. Note that only one incorrect classification is observed in both tables, and the corresponding overall correct recognition rate is $P_c = 279/280 = 99.64\%$. This result confirms that the previous assumption of the multivariate normal distribution of the training data set across the aspects is valid, and implies that the training features from different targets are well separated from each other in the feature space.

Tables IV and V show the confusion matrices of the proposed scheme replacing Step 1) in Section III with the conventional IFFT. The data set used for this experiment and associated parameters are the same as in the previous experiment. Note that the results in Tables II and III are improved over those of Tables IV and V due to the poor resolution of the IFFT.

B. Effect of Bandwidth

To investigate the performance of the proposed technique in terms of bandwidth, we performed the classification experiments using SET 1, and its bandwidth is varied from 2 to 4 GHz with a 1-GHz step. The selected bandwidths are 8.3–10.3 GHz, 8.3–11.3 GHz, and 8.3–12.3 GHz, and associated fractional bandwidths are 21.51%, 30.61%, and 38.83%, respectively.

TABLE IV
CONFUSION MATRIX OF THE IFFT USING SET 2 AND HH POLARIZATION.
THE SELECTED PARAMETERS ARE: BANDWIDTH = 8.3–12.3 GHz,
 $N = N_r = 401$, $p_{\max} = 20$ AND $l = 7$ (OVERALL CORRECT
RECOGNITION RATE $P_c = 97.86\%$)

Actual Class	Classification				
	Target-1	Target-2	Target-3	Target-4	Target-5
Target-1	54	2	0	0	0
Target-2	1	55	0	0	0
Target-3	0	0	55	1	0
Target-4	0	0	1	55	0
Target-5	0	1	0	0	55

TABLE V
CONFUSION MATRIX OF THE IFFT USING SET 2 AND VV POLARIZATION.
THE SELECTED PARAMETERS ARE: BANDWIDTH = 8.3–12.3 GHz,
 $N = N_r = 401$, $p_{\max} = 20$ AND $l = 7$ (OVERALL CORRECT
RECOGNITION RATE $P_c = 87.86\%$)

Actual Class	Classification				
	Target-1	Target-2	Target-3	Target-4	Target-5
Target-1	42	12	1	1	0
Target-2	6	43	4	0	3
Target-3	0	0	52	2	2
Target-4	0	0	2	53	1
Target-5	0	0	0	0	56

The polarization was chosen as VV. In addition, Step 1) in Section III was replaced with the IFFT, and the same classification experiments were performed. The results are shown in Fig. 6.

In Fig. 6, one can see that the performance of the proposed technique based on MUSIC or IFFT is very robust to the bandwidth variations. However, the results of the MUSIC are much superior to those of the IFFT due to its increased resolution for the same bandwidth.

C. Effect of Training Set Size

An efficient target recognition system should provide sufficient recognition accuracy even though the training set size is small. The small size of the training set implies that the training database can be efficiently compressed, and it provides significant advantages in terms of memory storage and computation speed.

Figs. 7 and 8 show the P_c values versus the training set size for the case of HH and VV polarizations, respectively. We used all three data sets in Table I, i.e., SET 1, SET 2, and SET 3, and selected the bandwidth to be 4 GHz. In Figs. 7 and 8, the proposed scheme, whether it is combined with MUSIC or with IFFT, is robust to the training set size, but the results of the MUSIC are superior to those of the IFFT. For the typical five targets used in this study, P_c values of the VV polarization are much more robust to the training set size than those of the HH polarization. From these figures, it is shown that the proposed technique combined with MUSIC can successfully identify different targets only using the training data set consisting of 13.33% of the overall data set.

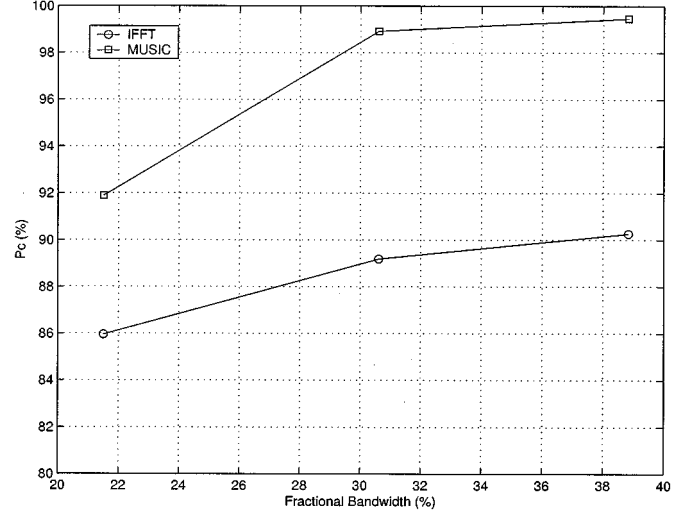


Fig. 6. P_c versus fractional bandwidth display using SET 1 and VV polarization. The parameters with a 2 GHz bandwidth: 8.3–10.3 GHz, $N = N_r = 201$, $m = 67$, $\hat{L} = 30$, $p_{\max} = 20$, and $l = 7$. The parameters with a 3 GHz bandwidth: 8.3–11.3 GHz, $N = N_r = 301$, $m = 100$, $\hat{L} = 30$, $p_{\max} = 20$, and $l = 7$. The parameters with a 4 GHz bandwidth: 8.3–12.3 GHz, $N = N_r = 401$, $m = 134$, $\hat{L} = 30$, $p_{\max} = 20$, and $l = 7$. The MUSIC and IFFT share the same parameters above, but the IFFT does not require the two parameters m and \hat{L} .

D. Effect of Additive Noise

To evaluate the performance of the proposed scheme in a noisy environment, the measured RCS in Fig. 3 was contaminated by AWGN to achieve the desired signal-to-noise ratio (SNR) from 0 to 40 dB with a 10-dB step. Note that the actual noise level contained in the data may be somewhat higher than the desired noise level since the measurement noise level was not considered in the process of noise addition. SET 1 with a 4-GHz bandwidth and HH polarization were used, and we performed ten Monte Carlo simulations using ten independent AWGN at each SNR. The resultant ten P_c s are averaged to obtain more reliable results.

Fig. 9 shows the result of the proposed technique combined with MUSIC. The error bars around estimated P_c values in Fig. 9 mark one (estimated) standard deviation above and below the estimated P_c values. The averaged P_c s decrease, and their standard deviations increase slowly with the decrease of SNR. P_c is larger than 60% even when SNR is 0 dB.

The result of the proposed technique combined with the IFFT is presented in Fig. 10. We observe that the estimated P_c values are significantly decreased for SNR levels below 20 dB, and their standard deviations are large. Comparing Figs. 9 and 10, it can be seen that the MUSIC algorithm is much more robust to noise than IFFT, and therefore has significant advantages in a noisy environment.

V. CONCLUSION

A new target recognition scheme based on range profiles has been proposed and analyzed. The proposed scheme utilizes the MUSIC algorithm and central moments features in addition to the appropriate preprocessing. The proposed features have translation and level invariance, which are essential to successful target recognition based on range profiles. The Bayes

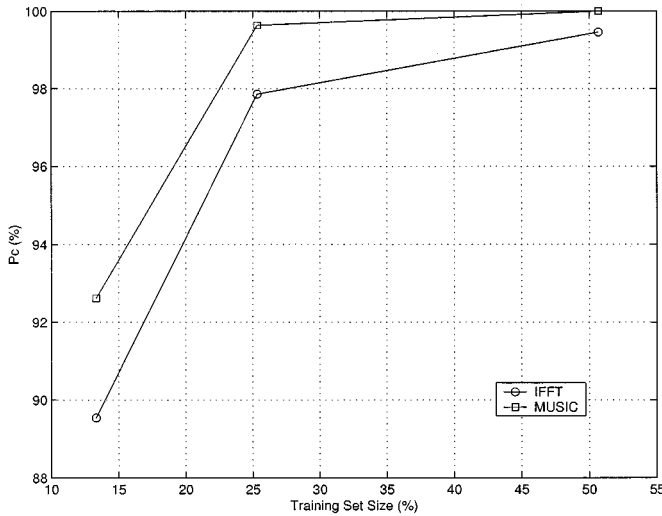


Fig. 7. P_c versus training set size display using SET 1, SET 2, SET 3, and HH polarization. The selected parameters for the MUSIC algorithm are: bandwidth = 8.3–12.3 GHz, $N = N_r = 401$, $m = 134$, $\hat{L} = 30$, $p_{\max} = 20$, and $l = 7$. The MUSIC and IFFT share the same parameters above, but the IFFT does not require the two parameters m and \hat{L} .

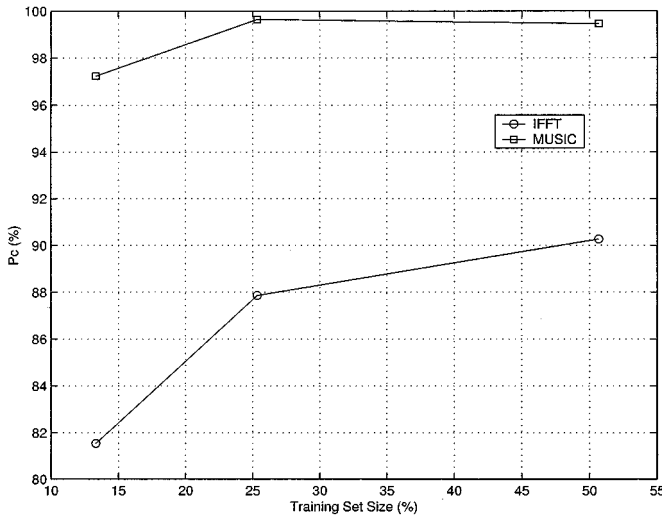


Fig. 8. P_c versus training set size display using SET 1, SET 2, SET 3, and VV polarization. The selected parameters for the MUSIC algorithm are: bandwidth = 8.3–12.3 GHz, $N = N_r = 401$, $m = 134$, $\hat{L} = 30$, $p_{\max} = 20$, and $l = 7$. The MUSIC and IFFT share the same parameters above, but the IFFT does not require the two parameters m and \hat{L} .

classifier recognizes target types using the proposed features, and the results show that the proposed scheme has significant advantages in radar target recognition. For the stable operation of the algorithm, we have derived a criterion for selecting subarray dimensions of the MSSP by considering three conflicting requirements such as resolution, decorrelation, and computation complexity. Moreover, in view of the bandwidth, training set size, and noise sensitivity, it was shown that the MUSIC algorithm outperforms the conventional IFFT at the cost of computation time. The efficiency of the proposed algorithm comes from two major facts: the superresolved range profiles caused by the MUSIC algorithm and small dimensional features caused by the central moments and PCA. It is well known

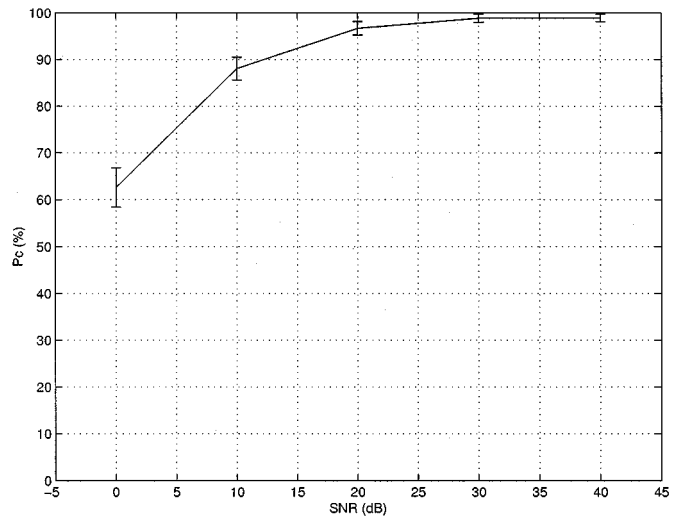


Fig. 9. P_c of MUSIC versus SNR display using SET 1 and HH polarization. The selected parameters for the MUSIC algorithm are: bandwidth = 8.3–12.3 GHz, $N = N_r = 401$, $m = 134$, $\hat{L} = 30$, $p_{\max} = 20$, and $l = 7$.

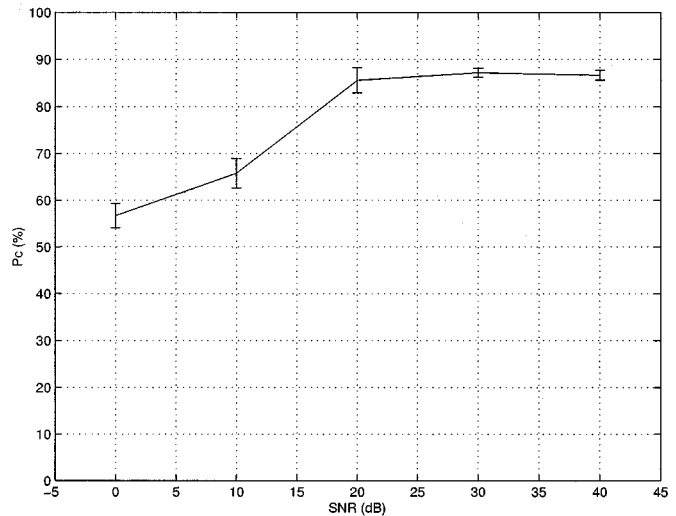


Fig. 10. P_c of the IFFT versus SNR display using SET 1 and HH polarization. The selected parameters for the IFFT are: bandwidth = 8.3–12.3 GHz, $N = N_r = 401$, $p_{\max} = 20$, and $l = 7$.

that range resolution is crucial to data compression across the angular domain and improvement of recognition accuracy. In addition, the small dimensional features can reduce memory storage and computation time during the classification stage.

The proposed technique in this paper can be combined with range profiles from other superresolution techniques, and combined with other classification techniques such as classical pattern classifiers and neural networks. These issues may be the area of future research.

REFERENCES

- [1] H. J. Li and S. H. Yang, "Using range profiles as feature vectors to identify aerospace objects," *IEEE Trans. Antennas Propagat.*, vol. 41, pp. 261–268, Mar. 1993.
- [2] D. L. Mensa, *High Resolution Radar Cross-Section Imaging*. Norwood, MA: Artech House, 1991.
- [3] D. R. Wehner, *High Resolution Radar*, 2nd ed. Boston, MA: Artech House, 1994.

- [4] E. Rothwell, D. P. Nyquist, K. M. Chen, and B. Drachman, "Radar target discrimination using the extinction-pulse technique," *IEEE Trans. Antennas Propagat.*, vol. AP-33, pp. 929–937, Sept. 1985.
- [5] K. M. Chen, D. P. Nyquist, E. J. Rothwell, L. L. Webb, and B. Drachman, "Radar target discrimination by convolution of radar returns with extinction pulses and single-mode extraction signals," *IEEE Trans. Antennas Propagat.*, vol. AP-34, pp. 896–904, July 1986.
- [6] J. E. Moony, Z. Ding, and L. S. Riggs, "Robust target identification in white Gaussian noise for ultra wide-band radar systems," *IEEE Trans. Antennas Propagat.*, vol. 46, pp. 1817–1823, Dec. 1998.
- [7] A. Moghaddar and E. K. Walton, "Time-frequency distribution analysis of scattering from waveguide cavities," *IEEE Trans. Antennas Propagat.*, vol. 41, pp. 677–680, May 1993.
- [8] L. C. Trintinalia and H. Ling, "Interpretation of scattering phenomenology in slotted waveguide structures via time-frequency processing," *IEEE Trans. Antennas Propagat.*, vol. 43, pp. 1253–1261, Nov. 1995.
- [9] H. Kim and H. Ling, "Wavelet analysis of radar echo from finite-sized targets," *IEEE Trans. Antennas Propagat.*, vol. 41, pp. 200–207, Feb. 1993.
- [10] E. J. Rothwell, K. M. Chen, D. P. Nyquist, J. E. Ross, and R. Bebermeyer, "A radar target discrimination scheme using the discrete wavelet transform for reduced data storage," *IEEE Trans. Antennas Propagat.*, vol. 42, pp. 1033–1037, July 1994.
- [11] Q. Li, E. J. Rothwell, K. M. Chen, and D. P. Nyquist, "Radar target discrimination schemes using time-domain and frequency-domain methods for reduced data storage," *IEEE Trans. Antennas Propagat.*, vol. 45, pp. 995–1000, June 1997.
- [12] A. Zyweck and R. E. Bogner, "Radar target classification of commercial aircraft," *IEEE Trans. Aerosp. Electron. Syst.*, vol. 32, pp. 598–606, Apr. 1996.
- [13] R. O. Schmidt, "Multiple emitter location and signal parameter estimation," *IEEE Trans. Antennas Propagat.*, vol. 34, pp. 276–280, Mar. 1986.
- [14] J. Capon, "High resolution frequency-wavenumber spectrum analysis," *Proc. IEEE*, vol. 57, pp. 1408–1418, Aug. 1969.
- [15] E. K. Walton, "Far-field measurements and maximum entropy analysis of lossy material on a conducting plate," *IEEE Trans. Antennas Propagat.*, vol. 37, pp. 1042–1047, Aug. 1989.
- [16] R. Carriere and R. L. Moses, "High resolution radar target modeling using a modified Prony estimator," *IEEE Trans. Antennas Propagat.*, vol. 40, pp. 13–18, Jan. 1992.
- [17] H. J. Li, Y. D. Wang, and L. H. Wang, "Matching score properties between range profiles of high-resolution radar targets," *IEEE Trans. Antennas Propagat.*, vol. 44, pp. 444–452, Apr. 1996.
- [18] H. Yamada, M. Ohmiya, Y. Ogawa, and K. Itoh, "Superresolution techniques for time-domain measurements with a network analyzer," *IEEE Trans. Antennas Propagat.*, vol. 39, pp. 177–183, Feb. 1991.
- [19] T. J. Shan, M. Wax, and T. Kailath, "On spatial smoothing for direction-of-arrival estimation of coherent signals," *IEEE Trans. Acoust., Speech, Signal Processing*, vol. ASSP-33, pp. 806–811, Aug. 1985.
- [20] M. Wax and T. Kailath, "Detection of signals by information theoretic criteria," *IEEE Trans. Acoust., Speech, Signal Processing*, vol. ASSP-33, pp. 387–392, Apr. 1985.
- [21] M. Wax and I. Ziskind, "Detection of the number of coherent signals by the MDL principle," *IEEE Trans. Acoust., Speech, Signal Processing*, vol. 37, pp. 1190–1196, Aug. 1989.
- [22] M.-K. Hu, "Visual pattern recognition by moments invariants," *IRE Trans. Inform. Theory*, vol. IT-8, pp. 179–187, Feb. 1962.
- [23] S. A. Dudani, K. J. Breeding, and R. B. McGhee, "Aircraft identification by moments invariants," *IEEE Trans. Comput.*, vol. C-26, pp. 39–45, Jan. 1977.
- [24] A. Khotanzad and J.-H. Lu, "Classification of invariant image representations using a neural network," *IEEE Trans. Acoust., Speech, Signal Processing*, vol. 38, pp. 1028–1038, June 1990.
- [25] S. Paschalakis and P. Lee, "Pattern recognition in grey level images using moment based invariant features," in *Inst. Elect. Eng. Image Processing and Its Applications*, Conference Pub. 465, 1999, pp. 245–249.
- [26] J. Flusser, T. Suk, and S. Saic, "Recognition of blurred images by the method of moments," *IEEE Trans. Image Process.*, vol. 5, pp. 533–538, Mar. 1996.
- [27] C. H. Jeh and R. T. Chin, "On image analysis by the methods of moments," *IEEE Trans. Pattern Anal. Machine Intell.*, vol. 10, pp. 496–511, July 1988.
- [28] S. Haykin, *Neural Networks*, 2nd ed. Englewood Cliffs, NJ: Prentice-Hall, 1999.
- [29] M. Friedman and A. Kandel, *Introduction to Pattern Recognition*, ser. Series in Machine Perception Artificial Intelligence: Imperial College Press, 1999, vol. 32.
- [30] J. W. Odendaal, E. Barnard, and C. W. I. Pistorius, "Two-dimensional superresolution radar imaging using the MUSIC algorithm," *IEEE Trans. Antennas Propagat.*, vol. 42, pp. 1386–1391, Oct. 1994.



Kyung-Tae Kim was born in Taejon, Korea, on April 15, 1970. He received the B.S., M.S., and Ph.D. degrees in electrical engineering from the Department of Electrical Engineering, Pohang University of Science and Technology (POSTECH), Pohang, Kyungbuk, Korea, in 1994, 1996, and 1999, respectively.

From March 1999 to March 2001, he worked at the Electromagnetics Technology Laboratory, POSTECH, as a Research Fellow. From April 2001 to February 2002, he worked as a Research Assistant Professor, Electrical and Computer Engineering Division, POSTECH. He is now on the faculty of the Department of Electrical Engineering and Computer Science, Yeungnam University, Kyongsan, Kyungbuk, Korea. His primary research interests include radar target recognition and imaging, array signal processing, spectral estimation, pattern recognition, neural networks, and RCS measurement and prediction.



Dong-Kyu Seo received the B.S. degree in electronic, electrical, and control engineering from Hongik University, Seoul, Korea, in 1999 and the M.S. degree from the Department of Computer and Communication Engineering, Pohang University of Science and Technology (POSTECH), Pohang, Korea, in 2001, where he is currently pursuing the Ph.D. degree in electrical engineering.

His research interests are in the areas of radar target imaging and recognition, radar signal processing, pattern recognition using artificial intelligence, and RCS measurement.



Hyo-Tae Kim received the B.S. and M.S. degrees in electronics engineering from Seoul National University, Seoul, Korea, in 1978 and 1982, respectively, and the Ph.D. degree in electrical engineering from The Ohio State University, Columbus, in 1986.

After his graduate work at the ElectroScience Laboratory, he joined the Faculty of Pohang University of Science and Technology, Pohang, Korea, where he is now a Professor. His research activity and interests are in the areas of antennas, EM scattering, EMI/EMC, and radar signal processing for imaging and identification.